Research Square

Preprints are preliminary reports that have not undergone peer review.
They should not be considered conclusive, used to inform clinical practice,
or referenced by the media as validated information.

Damage failure analysis of carbon fiber composite laminates under bending load

She Lingjuan

shelingjuan@zoomlion.com

Hunan University

Fu Ling

Zoomlion Heavy Industry Science and Technology Co., Ltd

Zhang Lei

Zoomlion Heavy Industry Science and Technology Co., Ltd

Long Xiangyun

Hunan University

Zhang Peng

Zoomlion Heavy Industry Science and Technology Co., Ltd

Yan Dulei

Zoomlion Heavy Industry Science and Technology Co., Ltd

Research Article

Keywords: composite material, bending load, failure criterion, progressive damage, numerical simulation

Posted Date: May 18th, 2026

DOI: https://doi.org/10.21203/rs.3.rs-9432224/v1

License: This work is licensed under a Creative Commons Attribution 4.0 International License.
Read Full License

Additional Declarations: No competing interests reported.

Damage failure analysis of carbon fiber composite laminates under bending load

She Lingjuan*[1,2,3], Fu Ling [2,3], Zhang Lei[2,3], Long Xiangyun[1], Zhang Peng[2,3], Yan Dulei[2,3]

1. College of Mechanical and Vehicle Engineering, Hunan University, Changsha, Hunan 410012, PR China
2. Zoomlion Heavy Industry Science and Technology Co., Ltd, Changsha, Hunan 410013, PR China
3. State Key Laboratory of Crane Technology, Changsha, Hunan 410013, PR China.
*Correspondence to: shelingjuan@zoomlion.com

ABSTRACT

The damage failure analysis of carbon fiber reinforced composite material (CFRP) main loading structure under the action of excessive bending load is extremely important. The traditional damage analysis methods have problems such as simple failure criterion, inapplicability of linear assumptions, and insufficient consideration of interlayer damage. To this end, this study uses the finite element simulation software as a platform to establish 3D models for simulating the damage characteristics of carbon fiber-reinforced composite laminates, and embeds the extended 3D Hashin failure criterion in the software subroutine to elucidate the phenomenon of intralaminar failure. The study adopts a bilinear traction-separation model to characterize the interlayer damage, and innovatively combines stress-damage analysis and experimental microscopic characterization, thus revealing the damage emergence mechanism and evolution law within the composite laminates under bending load. Taking 8-layer laminate as an example, the results of simulation analysis and experimental verification show that the calculation accuracy of the proposed model has been improved by 5%~10% compared with the traditional analysis method. The model has high computational accuracy for both the emergence and evolution of intra- and interlayer damage, which can provide an important theoretical basis and technical support for the design and optimization of CFRP components.

Keywords: composite material, bending load, failure criterion, progressive damage, numerical simulation

1.Introduction

Carbon fiber reinforced composite materials (CFRP) are widely used in structures such as aircraft skins, wind turbine blades, and thin-walled automotive components due to their excellent specific stiffness, specific strength, and fatigue performance [1,2]. Engineering machinery is one of the important application fields of carbon fiber composite materials, accounting for about 10%-15% of the global demand for carbon fiber composite materials. Carbon fiber reinforced composite material structures, due to their lack of reinforcement in the thickness direction, are susceptible to hard-to-detect delamination and crack defects. These defects significantly weaken the structural strength, leading to frequent safety accidents [3,4]. This shows that it is important to study the load carrying capacity and damage phenomena of composite materials. However, the physical detection of defects usually requires many samples and the operation is time-consuming and costly [4,5]. The development of reliable and accurate numerical simulation methods and the clarification of the

failure formation process can accurately predict the damage and residual strength of composite material structures [6,7]. Currently, traditional damage analysis methods have significant limitations in terms of the computational accuracy of complex failure modes, which are reflected in the simplicity of the failure criterion (linear or quadratic strength criterion), the inapplicability of linear assumptions, and the insufficient consideration of interlayer damage. CFRP has highly anisotropic and nonlinear behavior. Simple failure criteria are not effective in capturing the damage patterns of materials under multiple loads. In contrast to the conventional damage model, progressive damage means that the load is still carried according to a linear relationship before the failure criterion is reached, and after the failure criterion is reached, the load-carrying capacity of the laminates decreases rapidly. This method is widely used to characterize the damage behavior of composite materials [8,9]. Among them, Lin et al. [9] used progressive damage analysis to characterize the damage behavior of composite laminates. Xin et al. [10] proposed a progressive damage model for predicting the response and damage of fiber-reinforced plastic laminates under impact loading, and the simulation predictions matched well with the experimental results. Zhou et al. [11] adopted a multiscale progressive damage analysis method to research the damage behavior characteristics and strength prediction of two-dimensional planar braided composite materials under different loads, and the stress-strain curves matched well with the experimental results. Warren et al. [12] established a 3D progressive damage model to capture the onset and initial expansion of damage in 3D woven composite materials. Huai et al. [13] proposed an end-to-end time-space prediction model based on a progressive damage analysis method to predict delamination expansion of laminates under compressive loading. Guo et al. [14] established a progressive failure analysis finite element model for fiber reinforced polymer laminates to simulate the destruction and damage of composite laminates with a central hole under uniaxial tensile action. Huhne et al. [15] used the 3D Hashin failure criterion but did not consider the effect of interlayer damage. The above studies have shown that the progressive damage model is able to accurately predict the damage behavior within a laminate layer, but the problem of interlayer damage has not been well resolved. Most existing studies focus on the macroscopic characterization of intra-layer damage, and pay insufficient attention to the coupling effect of interlayer interfacial damage, especially the cross-scale behaviors such as delamination and interfacial debonding are often simplified as empirical criteria, resulting in a significant prediction bias of the damage evolution under complex loading.

Laminates are formed by laying and curing multiple layers of single-layer boards in a certain sequence, and their damage behavior includes intra-layer damage and interlayer damage. In terms of intra-ply damage, the Hashin failure criterion [16] is the most widely used criterion for intra-layer damage in composite laminates. Kirtunia et al. [17] developed a finite element model for a tensile specimen with a hole incorporating delamination, employing the three-dimensional Hashin failure criterion to numerically simulate intralaminar progressive damage. The average error between the experimental results and the finite element results was 4.2%. Ge et al [18] developed a finite element model for woven carbon fiber reinforced composite laminates under low-velocity impact, and the results showed that the developed numerical model can predict the dynamic response of the composite material better. In terms of interlayer damage, virtual crack closure technique (VCCT) based on fracture mechanics can only predict crack propagation, not crack initiation [19]. The cohesive zone method (CZM) creates special cohesive element s at the interface location to describe the mechanical behavior of the interface, predicting the location of damage initiation as well as the failure extension path in the absence of initial cracks [19,20,21]. Rezasefat et al. [23] used a bilinear traction-separation cohesion model by defining zero-thickness cohesion cells at the interface to account for interlayer damage in laminates under low-velocity impact. Zhao et al. [24] used cohesive element s (COH3D8) with a thickness of 0.01 mm thick placed between layers of double - double laminates for the study of type I delamination behavior. Xiao et al. [25] used progressive damage

analysis model, cohesive zone model and sandwich panel theory to establish a composite honeycomb sandwich panel model. Hongkarnjanakul et al. [26] inserted zero thickness cohesive element COH3D8 between fibers for simulating matrix cracking damage. Zou et al. [27] simulated the debonding and delamination of composite laminates under impact and compression by embedding cohesive elements within the reinforced composite laminates. The above studies have shown the effectiveness of introducing cohesive element s to simulate interlayer damage.

Existing studies are more focused on the flexural behavior of composite materials after being subjected to transverse compressive loading. In the actual design of load-bearing structures in engineering, the behavior of compression and other behaviors caused by bending is much more complicated, and the bending performance is an important index for the assessment of load carrying capacity [28]. Therefore, it is important to analyze the mechanical response of laminates under bending loads and to conduct an in-depth study on crack initiation and propagation under bending of laminates. In addition, most of the studies do not delve into the effect of microscale damage evolution on the macroscopic properties of sandwich structures.

For this purpose, a three-dimensional finite element model is established to simulate the damage behavior of carbon fiber-reinforced composite laminates. In this study, the three-dimensional Hashin failure criterion is adopted to formulate the intralaminar damage criteria, while the B-K criterion is incorporated to predict the interlaminar damage. This integrated progressive damage model is further compiled and embedded into a user-defined subroutine. On this basis, the study systematically analyzes the progressive damage evolution during the bending process of laminates and the stress redistribution characteristics after damage initiation. Moreover, industrial microscopy and scanning electron microscopy (SEM) are jointly employed to characterize the microstructural states of laminates and elucidate the underlying damage mechanisms.

2. Damage model

2.1 Intra-layer progressive damage model

The Hashin criterion [29-35] can accurately distinguish between fiber and matrix damage and identify four main failure modes, such as fiber tensile failure and matrix tensile failure, so it is widely used in finite element-based progressive damage analysis. The 3D Hashin failure criterion is embedded in the VUMAT subroutine to determine damage emergence. Meanwhile, in order to account for the effects of in-plane shear and out-of-plane shear, six failure modes are formed by expanding on the four failure modes.

Fiber stretching ($\varepsilon_{11} \geq 0$):

$$F_{ft} = (\frac{\varepsilon_{11}}{\varepsilon_{11T}})^2 \tag{1}$$

Fiber compression（$\varepsilon_{11} < 0$）:

$$F_{fc} = (\frac{\varepsilon_{11}}{\varepsilon_{11C}})^2 \tag{2}$$

Matrix stretching（$\varepsilon_{22} + \varepsilon_{33} \geq 0$）:

$$F_{mt} = (\frac{\varepsilon_{22}+\varepsilon_{33}}{\varepsilon_{22T}})^2 + (\frac{\gamma_{12}}{\gamma_{12f}})^2 + (\frac{\gamma_{13}}{\gamma_{13f}})^2 + \frac{\gamma_{23}^2-\varepsilon_{22}\varepsilon_{33}}{\gamma_{23f}} \tag{3}$$

Matrix compression（($\varepsilon_{22} + \varepsilon_{33} < 0$）:

$$\mathrm{F_{mc}} = \left(\frac{\varepsilon_{22}+\varepsilon_{33}}{2\gamma_{23\mathrm{f}}}\right)^2 + \frac{\varepsilon_{22}+\varepsilon_{33}}{\varepsilon_{22\mathrm{C}}}\left[\left(\frac{{\varepsilon_{22\mathrm{c}}}^2}{2{\gamma_{23\mathrm{f}}}^2}\right) - 1\right] + (\frac{\gamma_{12}}{\gamma_{12\mathrm{f}}})^2 + (\frac{\gamma_{13}}{\gamma_{13f}})^2 + \frac{\gamma_{23}^2-\varepsilon_{22}\varepsilon_{33}}{{\gamma_{23\mathrm{f}}}^2} \tag{4}$$

In-plane shearing (1-2 plane):

$$F_{ip} = (\frac{\gamma_{12}}{\gamma_{12f}})^2 \tag{5}$$

Out-plane shearing (1-3 and 2-3 planes):

$$F_{op} = (\frac{\gamma_{13}}{\gamma_{13f}} + \frac{\gamma_{23}}{\gamma_{23f}})^2 \tag{6}$$

Where 1, 2, and 3 represent the fiber direction (X), in-plane vertical direction (Y), and out-of-plane vertical direction (Z), respectively. F_{ft}, F_{fc}, F_{mt}, F_{mc}, F_{ip} and F_{op} are damage initiation parameters. When any of these parameters reaches 1, the damage initiation criterion is met, and stiffness degradation begins. ε_{11T} and ε_{11C} are the tensile and compressive failure strains in the fiber direction. ε_{22T} and ε_{22C} are the tensile and compressive failure strains in the matrix direction. γ_{ijf}(i,j=1,2,3, i≠j) is the shear failure strain.

When the aforementioned damage initiation criterion is satisfied, continuous loading will lead to a reduction in stiffness, which is manifested macroscopically as a reduction in the elastic modulus of the material, and a gradual reduction in the structural load carrying capacity. At this point, a suitable damage evolution model needs to be defined to simulate the damage accumulation process in the damaged region. Some scholars have adopted the energy method to analyze stiffness degradation [43,44,45]. This paper uses a simplified material stiffness degradation scheme, and the discounting scheme is shown in Table 1. In this case, different damage forms contribute differently to the material stiffness degradation, so different degradation coefficients are used for different damage modes.

Table 1 Mechanical properties

Damage mode	E_{11}	E_{22}	E_{33}	G_{12}	G_{23}	G_{13}
Fiber tensile	0.01	1	1	0.01	1	0.01
Fiber compression	0.01	1	1	0.01	1	0.01
Matrix tensile	1	0.01	0.01	0.01	0.01	0.01
Matrix compression	1	0.01	0.01	0.01	0.01	0.01
In-plane shear	1	1	1	0.01	1	1
Out-plane shear	1	1	1	1	0.01	0.01

Composite material layers can exhibit multiple damage modes at the same time, and the damage variables (d_{ft},d_{fc},d_{mt},d_{mc},d_{ip},d_{op}) are respectively related to the six damage modes, which are important parameters for describing the damage state. When its value is 0, it means that the material is not damaged. when its value is between 0 and 1, it means that the material is damaged to a certain extent. when its value is 1, it means that the material is completely damaged. Unlike conventional metallic materials, when composite materials are loaded, their energy absorption is mainly realized through the failure damage of the material, and this property of composite materials is characterized by element deletion during simulation. When element is deleted, the energy absorbed during the deformation of the element under load is also eliminated.

2.2 model of interlayer cohesion

In recent years, CZM (Cohesive zone model) has been widely used to predict the interface, adhesive and interlayer fracture behavior [30]. Compared to the virtual crack closure technique (VCCT), CZM can predict adhesive and interfacial damage initiation and evolution without and with initial cracks. Delamination damage in composite laminates initiates and propagates at the interface between two adjacent sublayers with different ply orientations. Therefore, the introduction of cohesion element s to locations where delamination is likely to occur can be effective in predicting the generation of delamination damage, damage propagation until the final delamination occurs. The three forms of interlayer damage are tension (type I), slip (type II), and misalignment (type III).The Cohesive cohesion element provided by Abaqus was used to simulate interlayer stratification. Quadratic nominal stress criterion (QNSC) was chosen as the damage initiation criterion [34,18,32] to predict the occurrence and extension of damage under hybrid loading. Damage occurs in the cohesive element when the sum of the squares of the nominal strain ratios in each direction is equal to 1, as follows:

$$\left\{\frac{\langle t_n \rangle}{t_n^0}\right\}^2 + \left\{\frac{t_s}{t_s^0}\right\}^2 + \left\{\frac{t_t}{t_t^0}\right\}^2 = 1 \tag{7}$$

where t_s, t_n and t_t represent normal and shear traction. t_n^0, t_s^0 and t_t^0 represent the peak nominal stresses at the interface in the normal and first/second shear directions, respectively [18]. The McCauley brackets $\langle\,\rangle$ indicate that the purely compressive state in the cohesive element does not cause any damage and only allows damage to occur when normal tensile traction is applied to the interface.

When damage begins to appear in the cohesive element , it is assumed that the damage evolves gradually according to a linear softening/degradation rule. The gradual decrease in stiffness here is triggered by the mixed-mode fracture energy criterion (BK energy criterion) proposed by Benzeggagh and Kenane [32]. The model is shown in Fig. 1 and equation (8):

$$G^C = G_n^C + (G_s^C - G_n^C)\left\{\frac{G_s^C+G_t^C}{G_n^C+G_s^C+G_t^C}\right\}^\eta \tag{8}$$

Where, G^C is the total critical energy. G_n^C, G_s^C and G_t^C are type I, type II, and type III fracture toughness (critical normal/shear fracture energy [32]), respectively. η is an empirical parameter obtained experimentally and depends on the modal ratio, interface ductility and loading rate.

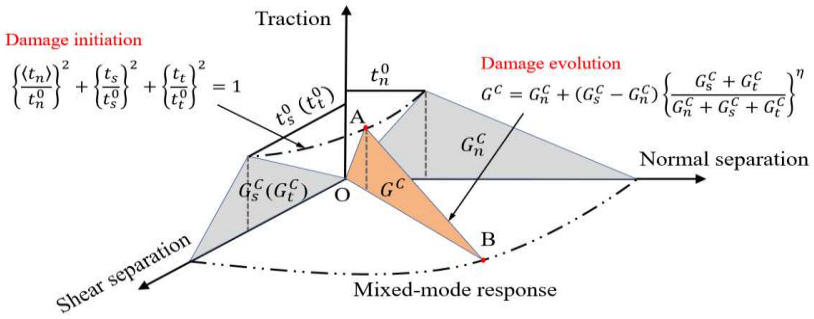


Fig.1 Bilinear traction-separation law of cohesive zone model

3.Numerical simulation

3.1 Constitutive model

The mechanical properties of each unidirectional layer in carbon fiber laminates can be described using the classical linear-elastic orthogonal anisotropic constitutive model. Three-dimensional constitutive modeling allows for better consideration of out-of-plane displacements. The stress and strain stiffness relationships for each cell of the orthotropic anisotropic material layer in the main material frame are:

$$\begin{bmatrix}\sigma_{11}\\ \sigma_{22}\\ \sigma_{33}\\ \tau_{12}\\ \tau_{23}\\ \tau_{31}\end{bmatrix}\begin{bmatrix} E_{11}(1-\nu_{23}\nu_{32})\Gamma & E_{11}(\nu_{21}+\nu_{31}\nu_{23})\Gamma & E_{11}(\nu_{31}+\nu_{21}\nu_{32})\Gamma & 0 & 0 & 0\\ E_{11}(\nu_{21}+\nu_{31}\nu_{23})\Gamma & E_{22}(1-\nu_{13}\nu_{31})\Gamma & E_{22}(\nu_{32}+\nu_{12}\nu_{31})\Gamma & 0 & 0 & 0\\ E_{11}(\nu_{31}+\nu_{21}\nu_{32})\Gamma & E_{22}(\nu_{32}+\nu_{12}\nu_{31})\Gamma & E_{33}(1-\nu_{12}\nu_{21})\Gamma & 0 & 0 & 0\\ 0 & 0 & 0 & G_{12} & 0 & 0\\ 0 & 0 & 0 & 0 & G_{23} & 0\\ 0 & 0 & 0 & 0 & 0 & G_{13}\end{bmatrix}\begin{bmatrix}\varepsilon_{11}\\ \varepsilon_{22}\\ \varepsilon_{33}\\ \gamma_{12}\\ \gamma_{23}\\ \gamma_{31}\end{bmatrix} \tag{9}$$

Where σ_{ij} (i,j=1,2,3)is the stress component. ε_{ij} (i,j=1,2,3) is the strain component. E_{ii} (i=1,2,3) is the tensile modulus. G_{ij} (i,j=1,2,3,$i \neq j$) is shear modulus. ν_{ij} (i,j=1,2,3, $i \neq j$) is the Poisson ratio. 1, 2, and 3 respectively represent the fiber direction, the in-plane vertical direction, and the out-plane vertical direction. Γ is defined in Eq. (10) and Poisson ratio and modulus of elasticity satisfy Eq. (11).

$$\Gamma = 1/(1-\nu_{12}\nu_{21}-\nu_{23}\nu_{32}-\nu_{13}\nu_{31}-2\nu_{21}\nu_{32}\nu_{13}) \tag{10}$$

$$\frac{\nu_{12}}{E_{11}}=\frac{\nu_{21}}{E_{22}},\frac{\nu_{13}}{E_{11}}=\frac{\nu_{31}}{E_{33}},\frac{\nu_{23}}{E_{22}}=\frac{\nu_{32}}{E_{33}} \tag{11}$$

The user-defined subroutine VUMAT is embedded in the finite element software Abaqus, and the progressive damage theory is adopted as the basic framework of the model, and the damage model and the stiffness degradation model from the previous paper are coded into the subroutine. The subroutine outputs SDV 1~6 are valid strains, and the output sequence is ε_{11}, ε_{22}, ε_{33}, γ_{12},

γ_{23}，γ_{13}. SDV7~14 are damage variables, SDV16~21 are damage coefficients, and when the damage coefficient reaches 1 then the damage variables change accordingly. The VUMAT subroutine needs to read the parameters from the software during the solution process and the results are returned to the software platform to complete the analysis of the model. The specific model flow is shown in Fig. 2.

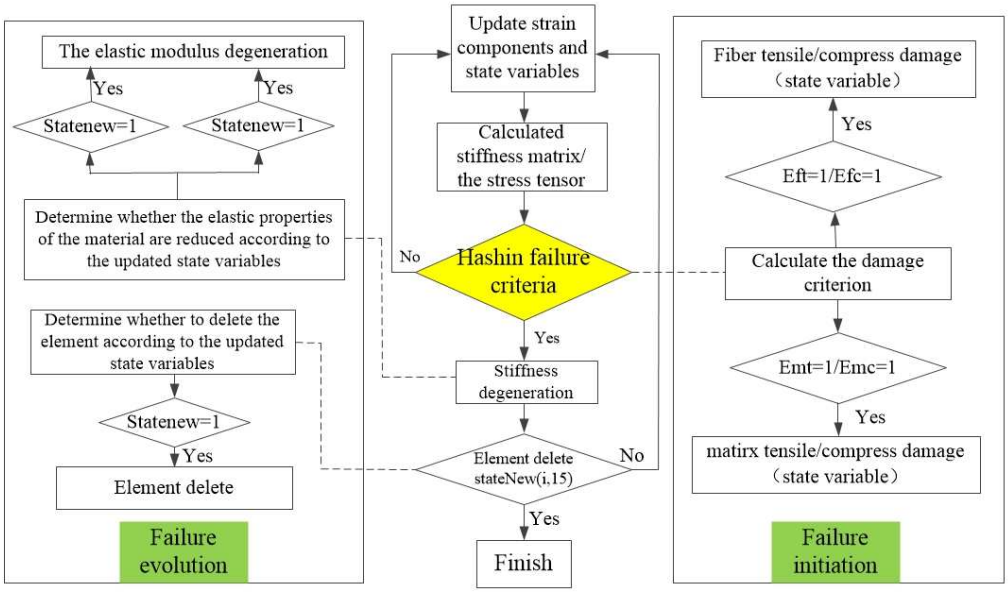


Fig. 2 Damage and failure flow chart based on VUMAT subroutine

The Cohesive element was used to simulate interlayer damage in composite laminates. The inter- layer material property parameters of carbon fiber composite laminates were obtained from Ref. [18] as shown in Table 2.

Table 2 Mechanical properties

Property	Symble	Value	Property	Symble	Value
Density (kg/m^3)	ρ	1596	Matrix tensile strength (MPa)	Y_T	50.8
Longitudinal modulus (GPa)	E_{11}	97	Matrix compressive strength (MPa)	Y_C	109
Transverse modulus (GPa)	E_{22}	10	Int-plane shear strength (MPa)	S_{12}	121
Out-plane modulus (GPa)	E_{33}	10	Out-plane shear strength (MPa)	S_{13}	121
Poisson's ratio v12	ν_{12}	0.3	Out-plane shear strength (MPa)	S_{23}	56
Poisson's ratio v12	ν_{13}	0.3	Cohesive stiffness(MPa)	K_n	3500
Poisson's ratio v12	ν_{23}	0.21		K_s=K_t	1346
In-plane shear modulus (GPa)	G_{12}	3.15	Nominal cohesive strength(MPa)	σ_n	20
Out-plane shear modulus (GPa)	G_{13}	3.15		σ_s=σ_t	34
Out-plane shear modulus (GPa)	G_{23}	4.32	Gritical fracture energy(kJ/m^2)	G_n^C	0.32
Fiber tensile strength (MPa)	X_T	1290		G_s^C	2.01
Fiber compressive strength (MPa)	X_C	534	B-K coefficient	η	2.09

3.2 Finite element model

Carbon fiber laminates were discretized into linear hexahedral solid elements of type C3D8R with enhanced hourglass control. Grid cells were established in the direction of the layup thickness for each layer of carbon fibers separately, and the interface phase between layers used the offset grid technique to establish zero-thickness cohesive COH3D8 cells. The cohesive zone cells shared the nodes of the neighboring solid cells in order to achieve the three-dimensional stress state of each cell. Finer grid cells were used in the loading region to improve the solution accuracy, and coarser grid cells are used in the peripheral region away from the loading to save computational cost. The mold is mesh discretized using S4R shell cells and given rigid body attributes. The user calls the for

file in Job-General before submitting the model and enables a double-precision solver.

3.3 Simulation analysis

A three-point bending finite element model was established in Abaqus with the laminate element and the mold element as shown in Fig. 3-a. The middle area element s are refined with a sheet thickness of 2.4mm, a length of 160mm, a width of 15mm and a span-to-thickness ratio of 32:1. The layers from top to bottom are respectively defined as ply-1 to ply-8. The four-node continuous element R3D4 is used for punches and supports. The laying method is [45, 0, -45, 90]. Each layer direction is defined using a local coordinate system. The local and global coordinate systems are shown in Fig. 3-b. The cells in the laminates conform to a three-way state of stress. If the fiber direction coincides with the X direction ($\sigma_{xx}=\sigma_{11}$), the stress state is simplified as in Fig. 3-b. At this time, the types of forces within the laminate face are positive stresses σ_{11} and σ_{22}, and shear force τ_{12}. Outside the surface are positive stresses σ_{33} and shear stresses τ_{13} and τ_{23}.

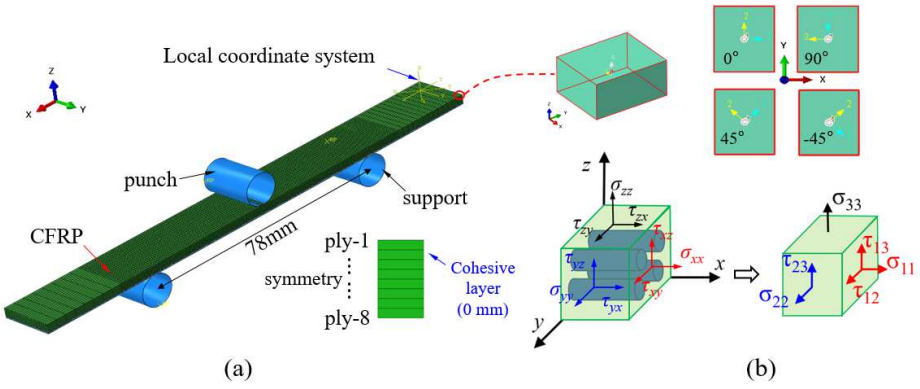


Fig. 3 Three point bending finite element model

3.3.1 Stress distribution

As the punch moves downward, the stress distribution in the laminate changes as shown in Fig. 4.

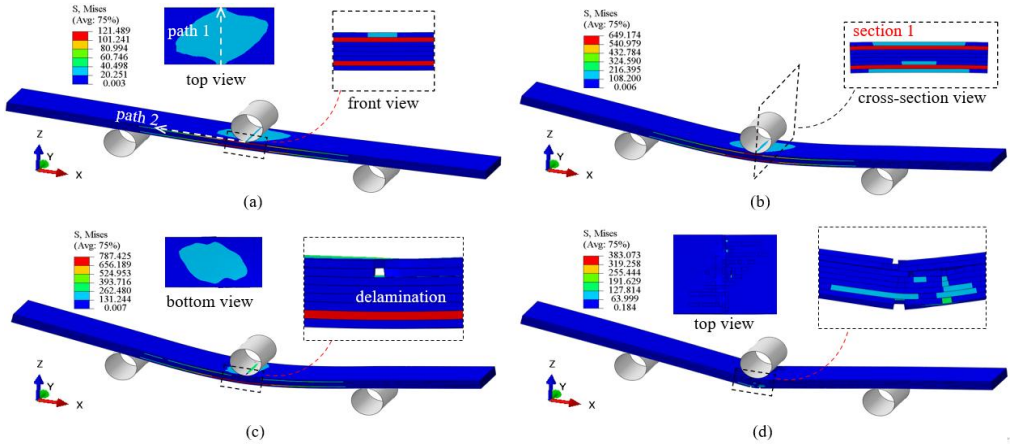


Fig.4 Strain distribution diagram of bending progress

As can be seen from Fig. 4-a, the surface stress distribution of the first 45° layer corresponds to the angle of its layup with an inclined distribution when the punch and the laminate are in contact. From the front view, it can be seen that the highest stresses are found in the second and seventh layers, which are 0° layers, and the direction of fiber reinforcement coincides with the direction of maximum deformation (X-direction). The neutral layer is subject to less tensile stress and is mainly subject to shear. For subsequent analysis, path1 along the Y direction and path2 along the -X direction are defined on the upper surface of the laminate as shown in Fig. 4-a. The intermediate section is defined as section1, as shown in Fig. 4-b. Fig. 4-c shows when the laminate is first damaged under load. From the front view it can be seen that element deletion occurs in the pressurized areas of the first and second layers and delamination defects occur between the layers.

Fig. 4-d shows the stress distribution after the punch continues to press down, and the top view shows the damage pattern distributed at a 45° angle, which shows the stress release of the laminate due to rupture. The overall stress value decreased significantly, with the maximum stress decreasing from 787 MPa to 383 MPa.

The layers are laid in different directions and are subjected to different forces within the loaded area. Therefore, the stress values of each layer at path-1 are extracted and the stress distribution is shown in Fig. 5-a below. In this case, the edge stress of ply-7 is higher than that in the middle region, the remaining layers exhibit the minimum stress at the edges, and the stress values of ply-2 and ply-7 are much greater than the other layers. The maximum and minimum principal stress distributions and their directions for section 1 are shown in Fig. 5-b and 5-c, where the second and seventh layers are subjected to the maximum compressive and tensile stresses, respectively.

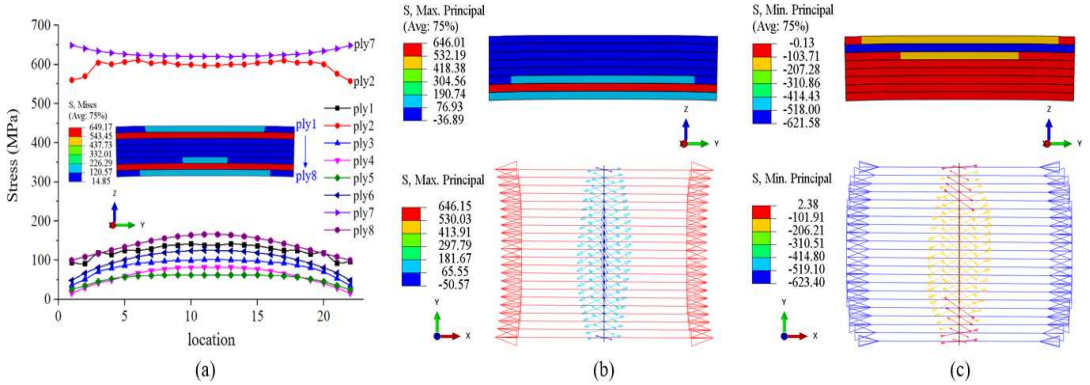


Fig. 5 Stress distribution on section-1

The stress distribution of CFRP laminates along the S11 and S22 directions is shown in Fig. 6. Among them, the direction S11 is parallel to the fiber direction and S22 is perpendicular to it. In the S11 direction, ply-1 and ply-8 are symmetric and share the same direction, while ply-1 is in compression and ply-8 is in tension. The maximum stress occurs at the central region of the loading area, and the distribution of 2 and 4, 7 and 5 is similar due to the same direction. The vertical fiber direction of 4 and 5 also agrees with the distribution pattern along the fiber direction of 2 and 7.

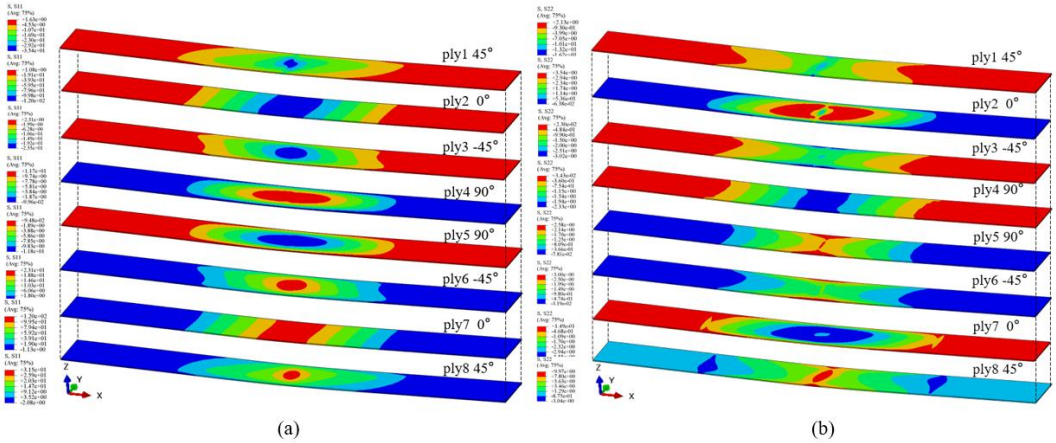


Fig. 6 Stress distribution for each ply (a)S11 and (b)S22

Fig. 7-a shows the curves of stress values versus displacement for eight elements in the thickness direction. Fig. 7-b shows the stress-time curves of elements uniformly distributed along Path2 (X-direction) at the center of the laminate's upper surface. At a punch displacement of 3.2 mm, the stress in the second layer element reaches a peak and the element subsequently fails. Its compressive stress along the fiber direction S11 = -552 MPa is close to the fiber compressive strength. The tensile stresses in the two directions perpendicular to the fiber are relatively small. When the punch subsequently reaches 4 mm, the tensile stress in the seventh layer element along

the fiber direction is S11 = 737.69 MPa, which does not reach the fiber tensile strength. This indicates that the sudden drop in stress is not due to the failure of the element , but rather to the breakage of the laminate, which releases the stress and thus affects the stress distribution in the laminate.

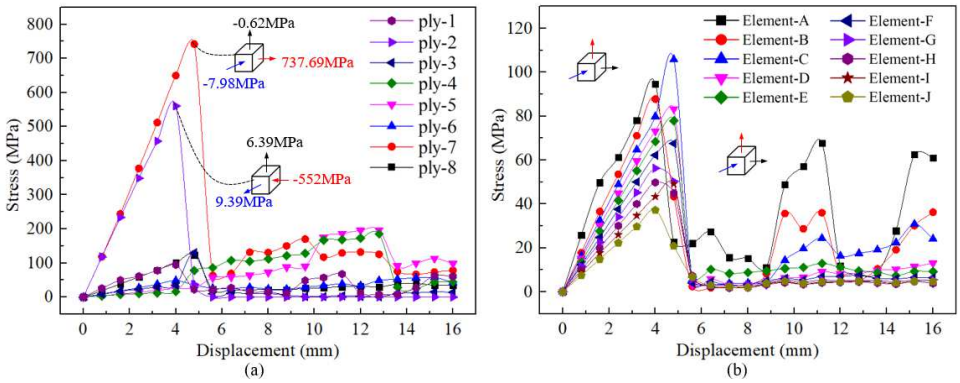


Fig. 7 (a) stress-displacement in the direction of thickness (b) stress-displacement curve along the path-2

The out-of-plane normal and shear stresses within the interlayer elements are induced by the tendency of adjacent layers to separate. Therefore, analyzing the forces acting on interlayer elements helps to identify the causes of delamination initiation. The zero-thickness cohesive element layer defined in Abaqus is a two-dimensional plane with no in-plane stresses. The distributions of S33, S13, and S23 stresses in the interlayer elements between Ply 1 (45°) and Ply 2 (0°) prior to damage initiation were visualized via post-processing, as shown in Fig. 8. The interlayer element layer is subjected to compressive stress in the Z-direction in the central region, which is caused by the downward pressure exerted by the punch. The S13 and S23 shear stresses exhibit central symmetry around the loading location, indicating that the out-of-plane shear stress distribution is closely related to the ply orientation. Interlayer shear stress is the primary cause of delamination in CFRP laminates [15,30].

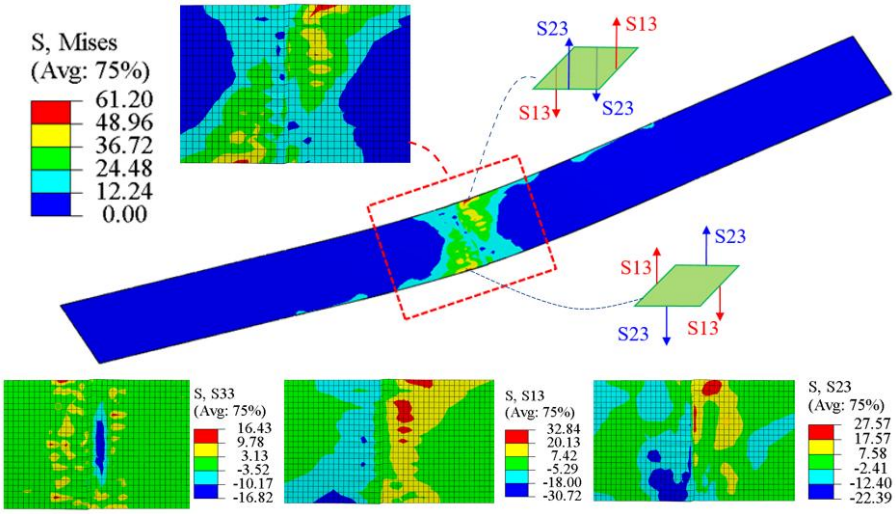


Fig. 8 Stress distribution of inter layer element

3.3.2 Damage distribution

Before damage occurred in the laminate, the damage distribution nephogram of each layer is shown in Fig. 9. A value of "1" (displayed in red in the nephogram) indicates that the corresponding failure mode has occurred at the specific position of the specimen.

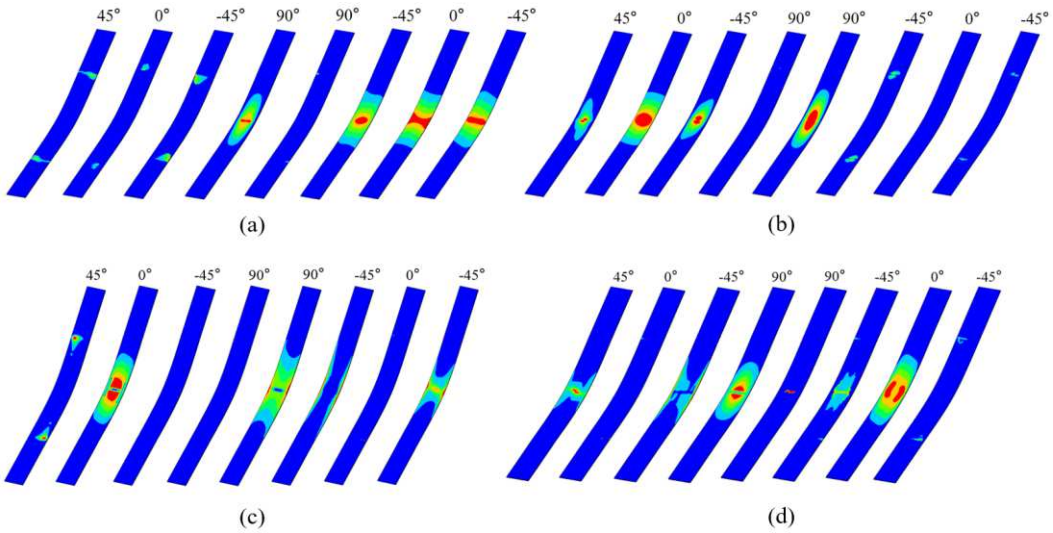


Fig. 9 Damage distribution of each layer (a) fiber tensile (b) fiber compress (c) matrix tensile (d) matrix compress

Fig. 9-a shows that the fiber tensile damage is centered at the bottom ±45° and 0° directions. Fiber tensile damage is present in ply-4 (90°) because the compressive stresses in the X-direction of this layer are taken up by the matrix (Fig. 9-d), and the compression of the element in the X-direction leads to Y-direction stretching.

From Fig. 9-b, it is clear that the fiber compression damage is concentrated in ply-1~3 and ply-5 layers. The maximum compressive deformation in the x-direction occurs at ply-1 (45°). Laminate forces along the 45 direction are carried by the fibers. The forces in the direction of the vertical fibers are carried by the matrix (Fig. 9-d). The fibers and matrix sustain varying degrees of compression damage.

Based on the results of the stress analysis, it is evident that ply-2 is subjected to compression in the x-direction. However, comparing Fig. 9-c and Fig. 9-d, it is found that the matrix tensile damage in the middle region of ply-2 is obvious, while the matrix compression damage is almost none. The reason is that the force in the X-direction of the layer is carried by the fibers, and the larger crush force in the X-direction leads to stretching in the Y-direction, and the tensile damage is reflected in the matrix. Both Ply-3 and ply-4 exhibit matrix compression damage, and the direction of damage distribution is correlated with fiber direction. Ply-3 is a -45° layer with matrix compression damage found along the material. Ply-4 is a middle layer and the x-direction is perpendicular to the fiber direction, and there is matrix compression damage in the middle region. The ply-5 X-direction coincides with the matrix direction of tension, and there is matrix stretching and compression in a middle small part of the region. In Ply-7, due to the presence of large fiber tensile damage and matrix damage similarly dominated by matrix compression.

The intra-ply damage distribution corresponds to the stress distribution, and the analysis of the stress distribution and damage distribution in each ply helps to trace the causes of localized damage in the laminate. The matrix tensile damage distribution of the extracted ply1~3 layers of the laminate is shown in Fig. 10. Blue color indicates that the element has not failed or been deleted, and red color indicates that the element is about to fail. The damage distribution of ply-1 (45°) is along the fiber direction and the force of ply-2 (0°) in the X direction is carried by the fiber. According to the three-way force of the element , it is known that the larger crush force in the X-direction leads to compression in the Y-direction, and the tensile damage of the matrix occurs after the tensile force reaches the tensile strength of the matrix. Damage to Ply3(-45°) occurs along the -45° direction. The distribution is more complex due to the combined influence of Ply-2 (0°) and ply4 (90°). It can be seen from the aforementioned results and Eq.(3) that the distribution of matrix damage is closely correlated with the orientation of fiber reinforcement.

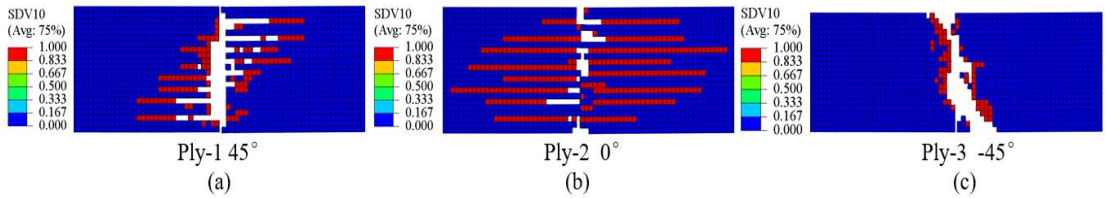


Fig. 10 Damage distribution of matrix tensile (a)ply-1 (b)ply-2 (c)ply-3

The damage distribution of the interlayer cohesive element is shown in Fig. 11. MMIXDMI characterizes the proportion of mixed fracture modes at initial damage and has a default value of -1 when the element is not damaged. A value of 1 indicates that complete shear damage has occurred, and a value of 0 indicates complete tensile damage.

From Fig. 11-a~b, it can be seen that the initial damage distributions at the interfaces between Ply 1 and Ply 2 (45° to 0°) and between Ply 2 and Ply 3 (0° to -45°) are affected by the layup mode, and both are dominated by shear damage. Among these, the interlayer between Ply 1 and Ply 2 exhibits 86.34% shear damage, with 4.54% tensile damage occurring in both the central region and the edges, and 9.12% mixed damage involving both modes. Fig. 11-c shows that there is very little interlayer damage between Ply 3 and Ply 4. The results show that the interlayer damage under bending load mainly occurs at the two interfaces on the compression side, and the interlayer damage is dominated by shear damage, and is highly correlated with the fiber layup method.

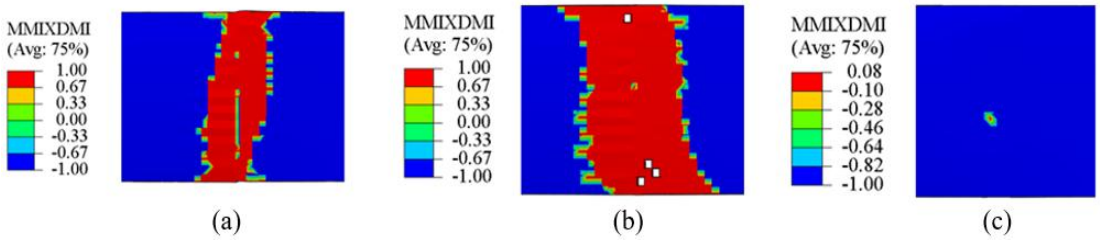


Fig. 11 Damage distribution of interfacial element (a)ply-1~2 (b)ply-2~3 (c)ply-3~4

4. Experimental verification

4.1 Material and sample preparation

The epoxy resin produced by Huibai New Material was used as the matrix material, and the unidirectional fiber cloth with a thickness of 0.3 mm was utilized as the reinforcing material, and the specimens were symmetrically laid in a layup sequence of [45, 0, -45, 90] . The unidirectional fiber cloth was first laid according to the predetermined layup sequence, with infusion and isolation cloths used to assist resin flow and demolding, and a plastic film applied externally to create a vacuum environment. The laminate was cured in a curing oven at a temperature of 70℃, and the bending specimens were obtained by cutting with an engraving machine.

4.2 Mechanical tests

Three-point bending tests were performed using the MTS CMT-5105 testing machine as shown in Fig. 12 (a). The test was performed according to ASTM D7264 with specimens cut to dimensions of 160 mm × 15 mm, a thickness of 2.4 mm, and a span-to-thickness ratio of 32:1. To improve accuracy, three samples were tested with a controlled test speed of 2 mm/min. An industrial microscope was used to observe the morphological characteristics of the specimens under bending load, while scanning electron microscope (SEM) was used to observe the micro-morphology of the fracture. Specific information can be found in Fig. 12 (b) and (c).

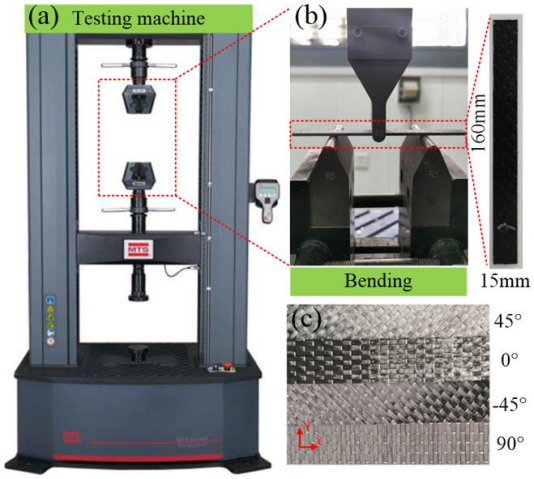


Fig. 12 Three-point bending test systems

4.3 Damage mechanism analysis

Fiber breakage is usually difficult to study experimentally [21]. Therefore, two methods of observing fiber breakage are used in this paper: a large drop in load (studied using force-displacement curves or force-time curves), and fiber-breakage cracks on the impacted surface (visually inspected). The damage morphology of the laminate after bending was observed with a high-definition industrial microscope and a scanning electron microscope, and damage mode analysis was performed on the laminates to reveal the complex damage mechanism of the laminate.

4.3.1 Bending response of laminates

In order to analyze the damage morphology of the laminate at different stages, specimen Sample-1 was stopped when a sudden load drop occurred and was used to observe the initial location of the critical damage. Specimen Sample-2 continued to be loaded after the sudden load drop until the punch displacement reached 15 mm, at which point the test was stopped; this specimen was used to observe the extension of subsequent damage and the development of other damage modes. Fig. 13-a illustrates the three-point bending load configuration and the locations of the support points. Fig. 13-b displays a cross-sectional image of the sample, and the deformation and defects in Sample 1 are not readily apparent. Fig. 13-c shows a schematic diagram of the fiber direction of the laminate cross-section.

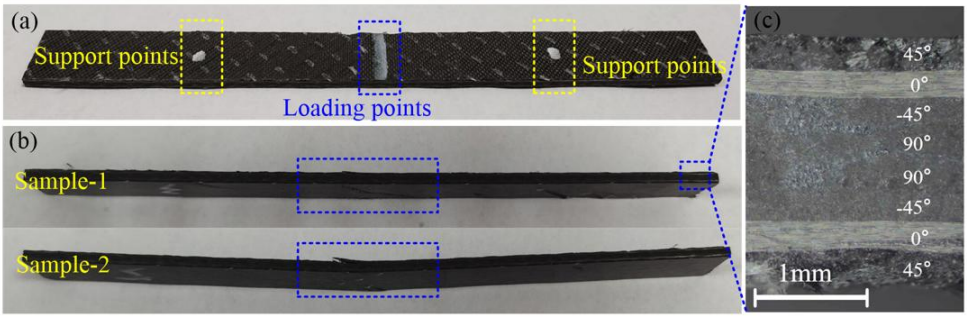


Fig. 13 Experimental results of bending samples

The load-displacement curves are shown in Fig. 14-a, where the curves of the three specimens overlap well. When the punch displacement reaches 5 mm, large fiber fracture leads to sudden change in load and a sudden drop in curve. After this, the laminate still has a certain load carrying capacity, and the simulation and experimental curves are close to each other, and the load carrying capacity is still close to each other after the fracture occurs. In the simulation, the load carrying capacity plummets again after the punch displacement exceeds 8 mm, which is different from the test results.

The experimental curve maintains a certain load-bearing capacity even in the failure stage,

which is associated with the complex strengthening mechanisms such as fiber bridging in multi-directional laminates [34]. However, this behavior cannot be accurately captured by the simulation model established in this study. Sample-1 of Fig. 14-b shows that the ply-1 and ply-2 layers are damaged near the loading point at the initial state of damage. Damage is presented as element deletion in finite element simulations. The ply-1 of Sample-2 cracked near the loading point along the 45° direction, while significant delamination occurred between ply-2~3. The reason for this is the concentrated compressive stress on the resin and fibers at the loading point during bending. Because the modulus of the resin is small and fails to transfer the load effectively, it cracks first under the action of concentrated compressive stress, and the direction of cracking is along the fiber direction. The experimental results coincide with the simulation results, which indicate that the finite element model can accurately simulate the bending deformation failure of laminates.

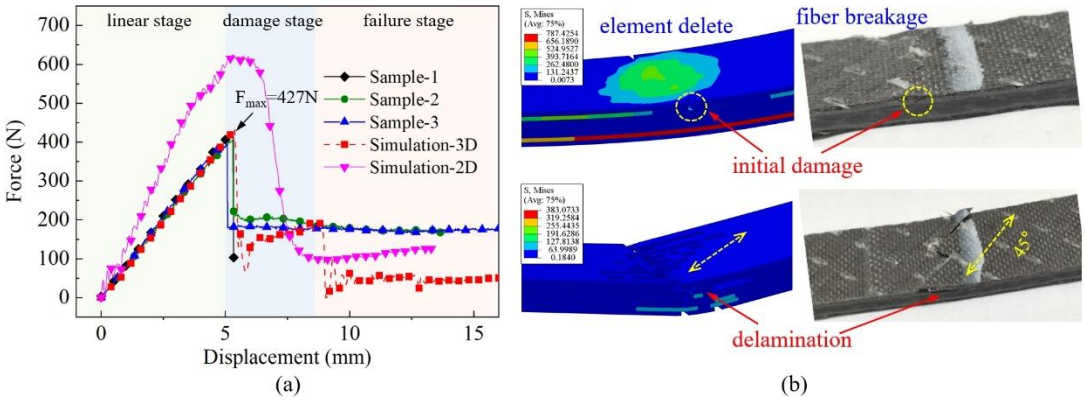


Fig. 14 Tensile test/simulation load-displacement curve

The lateral morphology of specimen Sample-1 in the first stage of bending is shown in Fig. 15-a. The damage area in the figure is concentrated near the loading point, and there is no significant damage in other areas.

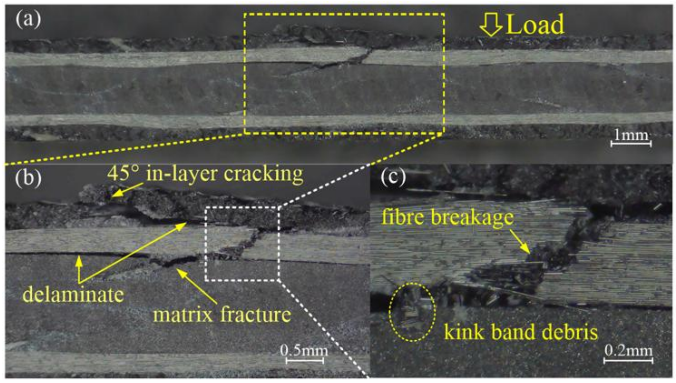


Fig. 15 Damage morphology of the first stage of bending

As shown in Fig. 15-b, the ply-2 layer (0°) fractured, and delamination damage occurred between both ply-1~2 and ply-2~3. Interlayer delamination and matrix rupture occur along the fiber fracture breaks between ply-2 and ply-3, and some of the matrix and fiber layers are still attached to the fiber layers with good adhesion. ply-3 locally appears to have an intralaminar matrix fracture as in Fig. 15-b, and is overall dominated by interlaminar damage. Twisted band debris can be found near the fracture, as shown in Fig. 15-c. With reference to Ref. [35], it is known that fibers form bending bands during flexure, and the characteristic fiber columns (twisted band fragments) can be observed at the fracture. The presence of kink bands can confirm the presence of fiber compression fractures. Fiber breakage, matrix cracking and interlayer delamination occur in the first stage of bending, resulting in a rapid decrease in the load-bearing capacity of the laminate.

In the second stage of bending (Sample-2), as shown in Fig. 16-a, the damage form becomes

more complex with continued bending. Fiber spalling of ply-1 and fiber breakage of ply-2 occurred on the left side of the load, and matrix fracture along the fibers occurred the 8th bottom layer. Fig. 16-b shows that fiber columns appear at fiber breaks and fiber bridging occurs between layers 2 and 3 [34]. Fig. 16-c is located directly below the load, with delamination defects occurring between ply-2 and ply-3 as well as multiple matrix failures. Matrix cracks extending along the thickness can be clearly seen, as well as cracks extending into the interlayer, thereby triggering delamination.

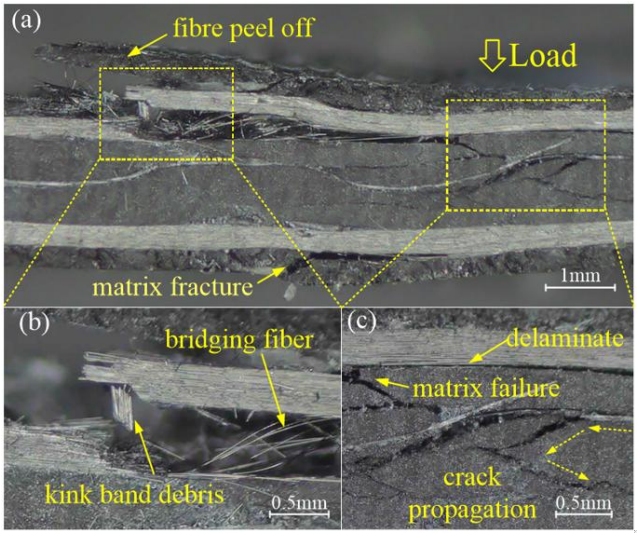


Fig. 16 Damage morphology of the second stage of bending

4.3.2 SEM morphology analysis

In order to deeply investigate the damage mechanism of laminates under bending load, model Prisma E scanning electron microscope (SEM) was used to observe the fracture morphology of the composite material along its thickness direction. In order to improve the image quality, a thin gold nanolayer was coated on the thickness surface of the sample using a model ETD-2000 ion sputtering instrument.

Fig. 17-a shows an undeformed cross-section of the laminate, which shows the different morphology of the layers of the multidirectional plate. Junction region A between Ply-2 and Ply-3 and localized region B of Ply-1 were selected for observation, as shown in Figs. 17-b and 17-c, respectively. Fig. 17-d shows the 200× morphology at the fiber fracture of Sample-1, which shows that the fiber section of ply-2 is relatively flat, and there are twisted band debris in the fracture region. The 500x magnification of the fracture region C and region D are respectively shown in Fig.17-e~f. Compared to Fig. 17-c, there are shear traces at the fiber bundle breaks in Figs. 17-e~f, where the latter fiber bundles are compressed with the bending of the laminate and then fail due to compressive stress. With reference to Ref. [37], it is known that two separate sections can be observed in the fiber bundle fracture. The side subjected to tensile stress will show a relatively flat cross-section, while the side subjected to compressive stress will show a shear failure cross-section that breaks diagonally, and the distribution of cross-section shapes within a region is relatively consistent. In addition, phenomena such as fiber detachment and interfacial debonding between fibers and matrix were observed in the fracture.

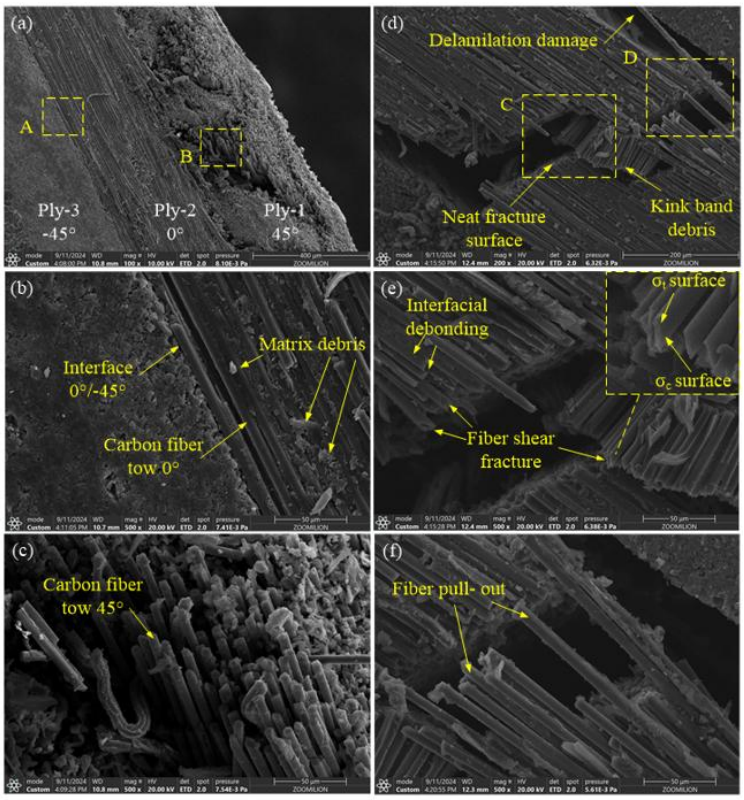


Fig. 17 SEM profile of curved section of Sample-1

Fig. 18 shows the cross-sectional morphology of Sample-2 and Sample-3. Fig. 18-a shows the fiber fracture of ply-2 (0°), where it can be seen that in the overall fiber break the surface is flat and some of the fibers are pulled out. Fig. 18-b shows matrix shear fracture of the ply-1 (45°) fiber layer, where fiber pullout and fiber debonding can be seen at the interface of ply-1 and ply-2. Fig. 18-c shows that delamination occurs between ply 7 to 8, and a matrix fracture along the 45° direction occurs at ply-8. Fig. 18-d shows the layered morphology between ply-1 and 2. Matrix fracture occurs at ply-1 (45°), indicating that the 45° layer is susceptible to matrix fracture due to intralayer shear under tension and compression. After the matrix of Ply-1 is damaged under load, matrix cracks extend to the interface between ply-1 and ply-2 layers, which leads to delamination defects. The ply-2 fibers continue to be subjected to compressive loading during bending after losing matrix support, and flexural fracture occurs after reaching the compressive strength of the fibers. Matrix microcracks excited by interlayer delamination can be observed in ply-3 in Fig. 18-e. The delamination interface between the Ply-2 to 3 layers is not flat, and part of the delamination is due to matrix fracture in the interior of ply-3. That is, the overall separation between fiber bundles which suggests that the interfacial strength here is greater than the shear strength inside ply-3 (45°). The shear crack morphology is evident in ply-4 and ply-5 in Fig. 18-f. The cracks propagated from ply-3~4 to ply-5~6, which indicated that the difficulty of interply and intralayer crack propagation was affected by the fiber lay-up method, and the cracks expanded fastest in the 90° ply (ply-3~4).

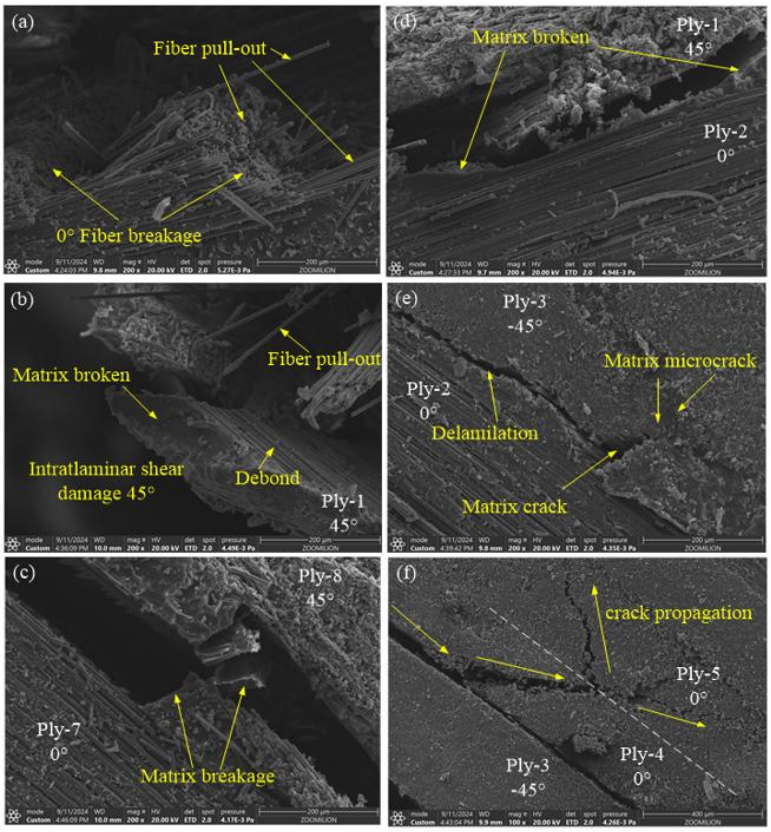


Fig. 18 SEM profile of curved section of Sample-2~3

Multidirectional laminates exhibit a variety of damage modes under bending loads, including fiber pullout, fiber fracture, matrix fracture, and weak interfaces leading to fiber debonding and delamination. Compression fracture of the Ply-2 fiber layer is the most important cause of laminate failure. The Ply-2 fibers release a large amount of energy after fracture, causing the surrounding matrix is broken, and the ply2~3 interlayers are violently sheared and deformed, thus leading to the initiation and propagation of the delamination. When the fiber is bent under pressure, due to the combined effect of tensile and compressive stresses, fractures occur on the side subjected to tensile load, leading to the formation of a 'bending band,' and ultimately, the damage is predominantly shear-dominated. In the “bending band” mode of destruction, the characteristics of the fiber columns can be observed microscopically at the fracture.

Under the bending load, each layer is subjected to different forces and the modulus difference between the resin and fiber is large, which is easy to cause concentrated shear stress at the interface between the fiber and resin and interlaminar shear damage, and thus transverse cracks are likely to occur due to delamination damage. Cracks are highly susceptible to penetration when encountering the 90° fiber layer, and are also more likely to penetrate the ±45° fiber layer and not the 0° fiber layer. The reason for this is that with the penetration of ± 45 ° and 90 ° fiber layer is mainly to destroy the interface between the fiber and the resin, the energy required is small. However, in the 0-fiber layer, due to the horizontal arrangement of the fibers, crack penetration is required to cut the fibers, which requires more energy.

5. Analysis and discussion of results

In order to further verify the scientificity and accuracy of the model proposed in this paper, the model and guidelines proposed in this paper are compared with the traditional damage analysis methods, and the comparison results are shown in Table 3.

Table 3 Results of method comparison

Index	VUMAT-based 3D Hashin Criterion[18]	Failure criterion for 2D Hashin[38,39]

Scope of application	Applicable to three-dimensional stress states, the failure behavior of composite materials under complex stresses can be more comprehensively analyzed.	It offers higher computational efficiency; however, it is only applicable to the two-dimensional plane stress state and cannot fully capture the failure behavior under three-dimensional stress conditions.
stress state	Consider all six stress components (σ_{11}, σ_{22}, σ_{33}, τ_{12}, τ_{13}, τ_{23}) to more accurately characterize material failure	Only the three in-plane stress components (σ_{11}, σ_{22}, τ_{12}) are considered, ignoring the effect of stresses in the thickness direction.
failure mode	Supports 6 independent failure modes	Single integral failure criterion
tolerance range	Higher prediction accuracy (5~10%) in complex stress states	Good performance in simple planar stress states, but insufficient prediction accuracy (10-20%) in complex stress states
damage evolution	Support for asymptotic nonlinear evolution	linear evolution

From Table 3, it can be found that the traditional 2D Hashin failure criterion usually considers only the in-plane stresses and strains and mainly analyzes the tensile, compressive, and shear failure modes, while the stress gradient in the thickness direction is neglected. For three-dimensional composite material structures, especially complex laminates, this simplified failure criterion fails to capture the failure modes under multidimensional stress states. This leads to low accuracy in damage prediction for laminates under complex loading. For example, damage and crack initiation occurring in the thickness direction cannot be effectively predicted in conventional models, which is critical in real-world engineering. Second, traditional damage analysis methods tend to rely on the linear assumption that the material maintains linear elastic behavior until the failure criterion is reached, which ignores the nonlinear properties of the material. Especially under multiaxial loading, the behavior of the composite material shows significant nonlinear characteristics, and the traditional methods cannot describe this process effectively. However, the 3D Hashin failure criterion proposed in this paper, combined with the progressive damage model, can take into account the nonlinear behavior of the material and gradually reduce the stiffness to simulate the damage accumulation process, thus achieving a more accurate damage evolution analysis. Finally, conventional methods usually ignore the complexity of interlaminar damage, especially when laminates are subjected to bending loads, where interlaminar damage (delamination and interfacial debonding) is an important factor affecting structural safety. Conventional models mainly focus on the simulation of intra-layer damage and cannot effectively predict the delamination behavior due to interlayer shear stress. The study combines the bilinear traction-separation cohesive zone model (CZM) and the 3D Hashin failure criterion, which can effectively take into account the coupling effect of interlayer-intralayer damages. It can effectively predict the initiation location of initial damage in large-scale, complex multi-directional laminates, and accurately predict the occurrence of delamination and interfacial debonding as well as their propagation processes.

In conclusion, the 3D Hashin failure criterion combined with the progressive damage model proposed in this paper has obvious advantages in simulating the damage evolution of carbon fiber composite laminates under bending loads. Compared with the traditional two-dimensional Hashin failure criterion, the proposed model not only comprehensively considers the three-dimensional stress state and accurately predicts the interlayer damage, but also simulates the nonlinear behavior of the material through the progressive damage model and captures the process of damage accumulation, thus significantly improving the accuracy and reliability of damage prediction. It can be observed that the damage modes such as fiber breakage, matrix compression damage and interlayer delamination, which occur in the bending process of laminates, are accurately simulated in the simulation, which verifies the feasibility and accuracy of the model in practical engineering application. It should also be clarified that, as indicated by the experimental results, factors such as material heterogeneity, randomness of spatial structure and complex nonlinear behavior of matrix

materials inside the laminates [36,37] all belong to micro-scale failure physical phenomena. Constrained by the scale and modeling methodology, the macroscopic simulation model adopted in this study cannot accurately characterize the aforementioned micro-scale features, thus exhibiting certain limitations. However, such limitations do not compromise the applicability of the model in practical engineering scenarios.

6. Conclusion

In this paper, the 3D finite element model for simulating the damage of carbon fiber reinforced composite laminates is established. This paper utilizes the 3D Hashin failure criterion to construct a damage criterion, combines it with the B-K criterion to predict the layered damage, and programs this progressive damage model into a user-defined subroutine. The progressive damage in the bending process of the laminate is analyzed, along with the stress redistribution after the occurrence of the damage, and the main conclusions of the joint industrial microscope and SEM scanning electron microscope study on the microscopic state of the laminate and the damage mechanism are as follows:

1）This progressive damage simulation model can accurately analyze the progressive damage behavior of laminates, characterize the initiation of initial damage in the form of element deletion and predict the delamination.

2）Failure of laminates under bending loads can be divided into two stages. Cracks appear along the fiber direction on the compression side in the first stage, and compression fracture occurs in the second 0° layer, which results in the loss of the main load-bearing capacity of the laminate. The second stage delamination crack extends along the resin matrix to other layers in delamination migration failure behavior.

3）Laminate in the bending load to form a ‘bending band’, the local appears fiber bridging phenomenon. Horizontal cracks occur as a result of delamination damage during interlayer shear. Because the interfacial bond between fiber and resin is weaker than the shear strength of the fiber, cracks can easily penetrate the 90° and ±45° fiber layers.

Data availability

Data will be made available on request. If necessary, please contact She Lingjuan (shelingjuan@zoomlion.com).

References

[1] Qihui Lyu, Ben Wanga, Zhenqiang Zhao, et al. Damage and failure analysis of hybrid laminates with different ply-stacking sequences under low-velocity impact and post-impact compression[J]. Thin-Walled Structures, 2022, 180, 109743.

[2] F. Cepero-Mejías, J.L. Curiel-Sosa, A. Blázquez, et al. Review of recent developments and induced damage assessment in themodelling of the machining of long fibre reinforced polymer composites [J]. Composite Structures, 2020, 240: 112006.

[3] O. Tanay Topac, Burak Gozluklu, Ercan Gurses, et al. Experimental and computational study of the damage process in CFRPcomposite beams under low-velocity impact[J]. Composites: Part A, 2017, 92: 167-182.

[4] Bin Yang, Yuan Chen, Juhyeong Lee, et al. In-plane compression response of woven CFRP composite after low-velocity impact: Modelling and experiment[J]. Thin-Walled Structures, 2021, 107186.

[5] Haibao Liu, Brian G. Falzon, Wei Tan. Predicting the Compression-After-Impact (CAI) strength of damage-tolerant hybrid unidirectional/woven carbon-fibre reinforced composite

laminates[J]. Composites: Part A, 2018, 105: 189-202.
[6] Wenhong Ao, Weimin Zhuang, Bobin Xing, et al. Finite element method of a progressive intralaminar and interlaminar damage model for woven fibre laminated composites under low velocity impact[J]. Materials & Design, 2022, 223, 111256.
[7] Alvaro Gonzalez-Jimenez, Andrea Manes, Alessio Beligni, et al. Modelling and Experimental Testing of Thick CFRP Composites Subjected to Low Velocity Impacts[J]. Procedia Structural Integrity, 2019, 24: 101-109.
[8] Anton Shipsha, Magnus Burman. Failure mechanisms in NCF composite bolted joints: Experiments and FE model[J]. 2020, 192, 107950.
[9] Lin Qingyuan, Yong Zhao, Chen Yan, et al. Progressive bearing failure analysis and strength prediction method for the initial assembly and tensile process of composite bolted joints[J]. 2024, 187, 108476.
[10] S.H. Xin, H.M. Wen. A progressive damage model for fiber reinforced plastic composites subjected to impact loading[J]. International Journal of Impact Engineering, 2015, 75: 40-52.
[11] Yuan Zhou, Zixing Lu, Zhenyu Yang. Progressive damage analysis and strength prediction of 2D plain weave composites[J]. Composites: Part B, 2013, 47: 220-229.
[12] Kyle C. Warren, Roberto A. Lopez-Anido a, Senthil S. Vel, et al. Progressive failure analysis of three-dimensional woven carbon composites in single-bolt, double-shear bearing[J]. Composites: Part B, 2016, 84: 266-276.
[13] Huai Yan, Weihua Xie, Bo Gao, et al. A spatiotemporal prediction model for rapid prediction of delamination growth in open-hole composite laminates[J]. Composites Science and Technology, 2023, 235: 109973.
[14] Zhangxin Guo, Hao Zhu, Yongcun Li. Simulating initial and progressive failure of open-hole composite laminates under tension[J]. Appl Compos Mater, 2016, 23: 1209-1218.
[15] Hühne C, Zerbst AK, Kuhlmann G,et al. Progressive damage analysis of composite bolted joints with liquid shim layers using constant and continuous degradation models[J]. Compos Struct, 2010, 92(2): 189-200.
[16] Z. Hashin. Failure criteria for unidirectional fiber composites[J]. Journal of Applied Mechanics, 1980,47, 329.
[17] Kirtunia Rahul, Arief Yudhanto, Pruthul Kokkada Ravindranath et al. Progressive damage modeling in open hole composite laminates with ultrasound-informed drilling-induced delamination[J]. Composites: Part A, 2024, 184, 108262.
[18] Xinxin Ge, Pan Zhang, Fei zhao, et al. Experimental and numerical investigations on the dynamic response of woven carbon fiber reinforced thick composite laminates under low-velocity impact[J]. Composite Structures, 2022, 279, 114792.
[19] Ala Tabiei, Wenlong Zhang. Composite laminate delamination simulation and experiment: a review of recent development[J]. Applied Mechanics Reviews, 2018, 70, 030801.
[20] Evren Sonat, Sezer Özerinç. Failure behavior of scarf-bonded woven fabric CFRP laminates[J]. Composite Structures, 2021, 258, 113205.
[21] Ligang Sun, Ying Tie, Yuliang Hou, et al. Prediction of failure behavior of adhesively bonded CFRP scarf joints using a cohesive zone model[J]. Engineering Fracture Mechanics, 2020, 228, 106897.
[22] Alvaro Gonzalez-Jimeneza, Andrea Manesa, Alessio Beligni, et al. Modelling and experimental testing of thick CFRP composites subiected to low velocity impacts[J]. Procedia Structural

Integrity, 2019, 24, 101-109.
[23] M. Rezasefat, Alvaro Gonzalez-Jimenez, M. Giglio, et,al. Numerical study on the dynamic progressive failure due to low-velocity repeated impacts in thin CFRP laminated composite plates[J]. Thin-Walled Structures, 2021, 167, 108220.
[24] Menglin Zhao, Yang Zhao, Anyang Wang, et al. Investigation of the mode-I delamination behavior of Double-Double laminate carbon fiber reinforced composite[J]. Composites Science and Technology, 2024, 248, 110463.
[25] Wen Xiao, Ganggang Sha, Xiaohua Lua, et al. Compressive failure analysis of composite honeycomb sandwich panels with impact damage and stepped-scarf repairs[J]. Thin-Walled Structures, 2024, 201, 112012.
[26] N. Hongkarnjanakul, C. Bouvet, S. Rivallant. Validation of low velocity impact modelling on different stacking sequences of CFRP laminates and influence of fibre failure[J]. Composite Structures, 2013, 106, 549-559.
[27] Jianchao Zou, Zhenkun Leia, Ruixiang Bai, et al. Damage and failure analysis of composite stiffened panels under low-velocity impact and compression after impact[J]. Composite Structures, 2021, 262, 113333.
[28] Wang Yichao, Li Peng, Zhou Juping. Influence of span—to—thickness ratio on the three—point bending behavior of carbon fiber composites [J]. Composites Science and Engineering, 2023, 3, 83-88.
[29] Fan Dong, Yazhi Li, Xin Qi, et al. Failure behavior and damage model of composite sandwich panels under three-point bending fatigue load[J]. Thin-Walled Structures, 2024, 205, 112570.
[30] Chunxing Hu, Zhonghai Xu, Xiangjun Liu, et al. An insight into the mechanical behavior and failure mechanism of CFRP/Al adhesively bonded structures subjected to low-velocity impact[J]. Engineering Fracture Mechanics, 2023, 294: 109733.
[31] Wen Xiao, Ganggang Sha, Xiaohua Lu, et al. Compressive failure analysis of composite honeycomb sandwich panels with impact damage and stepped-scarf repairs[J]. Thin-Walled Structures, 2024, 201: 112012.
[32] M.L.Benzeggagh, M. Kenane. Measurement of mixed-mode delamination fracture toughness of unidirectional glass/epoxy composites with mixed-mode bending apparatus[J]. Composites Science and Technology, 1996, 56(4): 439-449.
[33] Wushuai Liu, Fen Yu, Zhenpeng He, et al. A progressive damage model introducing temperature field for bolted composite joint with preload[J]. Modelling and Simulation in Materials Science and Engineering, 2019, 27: 065011.
[34] Zhao L B, Gong Y, Zhang J Y. A survey on delamination growth behavior in fiber reinforced composite laminates [J]. Acta Aeronautica et Astronautica Sinica, 2019, 40(1), 522509.
[35] Wang Han. Failure analysis of carbon fiber laminated composites for automotive applications [D]. Shanghai: Donghua University, 2023.
[36] Transverse failure prediction of unidirectional carbon fiber reinforced polymer composites subjected to uniaxial and biaxial loading by stress-triaxiality-dependent computational micromechanics[J]. Composite Structures, 2024, 345: 18359.
[37] Multiscale modeling framework to predict the low-velocity impact and compression after impact behaviors of plain woven CFRP composites[J]. Composite Structures, 2022, 299: 116090.
[38] 2D and 3D Finite Element models for the edge trimming of CFRP[J]. 16th CIRP Conference

on Modelling of Machining Operations, 2017, 233-238.
[39] Enhancing compressive failure prediction in repaired composites A comparative study of 2D and 3D Hashin criteria with experimental validation[J]. Thin-Walled Structures, 2025, 217, 113911.
[40] A damage threshold prediction model of CFRP panel by hail impact based on delamination mechanism[J]. Engineering Fracture Mechanics, 2020, 239: 107282.
[41] Residual crashworthiness of braided composite tube with transverse multi-impact damages: Experimental and numerical study[J]. Composite Structures, 2021 255: 112903.
[42] A review of methods for improving interlaminar interfaces and fracture[J]. Materials Today Communications, 2020, 22: 100830.
[43] Assessment of Ply Stacking Sequence Effect on Damage Behavior of CFRP Composite Laminate Under Low-Velocity Impacts [J]. Materials Today Communications, 2025, 21: 4349535.
[44] Blast analysis of efficient honeycomb sandwich structures with CFRP Steel FML skins[J]. International Journal of Impact Engineering, 2023, 1778: 104609.
[45] Reliability assessment of glass epoxy composite plates due to low velocity impact[J]. Composite Structures, 2018, 200: 659-688.

Author contribution statement

Lingjuan She: Data prediction, Model solution, Analysis Validation, Methodology, Writing. Ling Fu: Conceptualization, Investigation, Methodology, Supervision, Writing. Lei Zhang and Xiangyun Long: Methodology, Supervision. Peng Zhang and Dulei Yan: Information of crane acquisition.

Additional information

Declaration of competing interest

The authors declare that they have no known competing financial interests or personal relationships that could have appeared to influence the work reported in this paper.

Formatting of funding sources

Funding: This work was supported by Project supported by the National Key Research and Development Program of China [grant numbers 2024YFB3411100, 2023YFB3408500].